Operation Principles for Optical Switches Based on Two Multimode Interference Couplers

Junhe Zhou and Philippe Gallion, *Senior Member, IEEE*

***Abstract*—In this paper, the operation principles for optical switches based on two multimode interference (MMI) couplers are discussed in detail. Based on the analytical expressions of transfer matrix of the MMI couplers, the control mechanism and principles of the two-stage MMI coupler based switch are derived. The device can be controlled by proportionally adjusting the interstage variable phase shifter array. N different switching states can be realized on this device.**

***Index Terms*—MMI coupler, optical switch.**

I. Introduction

OPTICAL communication networks have evolved into the era of all optical switching and various approaches to realize all optical switches have been proposed. The MEMS switch [1], the liquid crystal based switch [2], the directional coupler based switch [3], the thin film based switch [4] and the MMI coupler based switch [5]–[7] have been either commercially available or realized in laboratories. In comparison with other optical switches, the MMI coupler based switch has the advantages of smaller size, greater feasibility for integration, and the capability of thermal-optical and electro-optical tuning. More attentions have been placed on this novel switching technology and recently there have been significant progresses in this field. In [5], F. Wang *et al.* proposed a 2×2 optical switch based a MMI coupler and realized it experimentally. L Cahill proposed the generalized structure for a cascaded-MMI-coupler based switch in [6], [7]. N different states of the switch were discussed in detail when N equals 4. In [8], a 4×4 MMI coupler based switch was experimentally fabricated and demonstrated.

Despite these pioneering works, the development of MMI coupler based switch still requires a comprehensive theoretical model in order to characterize its operation principles. With such a model, we will know how to operate the device in an optimal manner.

In this paper, based on the theory of the transfer matrix of the MMI couplers [9]–[12], the operation principles of MMI coupler based switches will be provided with the assistance of the analytical expressions. Totally N different states of the switch can be realized by proportionally tuning the variable phase shifter array in the middle of two MMI couplers. Simulations are performed to verify these operation principles. It is worth mentioning that the number of the states can be increased if the switches are operated in a cascaded manner, as is indicated by [7]. Detailed numerical simulation will be provided to verify our proposals.

Manuscript received July 12, 2011; revised September 30, 2011, November 12, 2011; accepted November 21, 2011. Date of publication November 30, 2011; date of current version January 06, 2012. This work was supported in part by the Fundamental Research Funds for the Central Universities of China.

J. Zhou is with the Deptartment of Electronics Science and Engineering, Tongji University, Shanghai 200092, China (e-mail: jhzhou@tongji.edu.cn).

P. Gallion is with TELECOM ParisTech and CNRS UMR 5141LTCI, Paris 75013, France (e-mail: philippe.gallion@telecom-paristech.fr).

Color versions of one or more of the figures in this paper are available online at http://ieeexplore.ieee.org.

Digital Object Identifier 10.1109/JLT.2011.2177812

II. Theory

A. MMI Coupler Transfer Matrix Theory [9]–[12]

MMI coupler works as a self-imaging device and can be characterized by the transfer matrix theory [9]–[12]. With this theory, the analytical relationship between the input vector and the output vector can be obtained.

To achieve the required transfer matrix, the positions of the input and output ports of the MMI coupler should be set carefully, so are the length and the width of the MMI coupler. Like [9], [10], the center of the input/output waveguides are placed at the position of

$$x_i = \left(i - \frac{1}{2}\right)\frac{W_e}{N} \quad (i = 1 \ldots N) \tag{1}$$

where W_e is the effective width of the MMI coupler, N the number of input/output. The length of the MMI L_N is set to be [10]

$$L_N = \frac{4 n_{\text{eff}} W_e^2}{N \lambda_0} \tag{2}$$

where n_{eff} is the effective index of the MMI coupler, λ_0 the free space wavelength. With the above configuration, the transfer matrix, which indicates the relationship between the input vector and the output vector, can be derived as [9], [12]

$$M_{lk} = (-1)^{l+k} j \exp\left(j\frac{\pi}{4}\right) \times \sqrt{\frac{1}{N}} \exp\left(-\frac{j((l-1/2) - (-1)^{l+k}(k-1/2))^2 \pi}{4N}\right) \tag{3}$$

where M_{lk} stands for the (l, k) entry of the transfer matrix. The validity of the transfer matrix theory can be proved by the comparison with the results obtained by [12], which gives the accurate information of the phase difference between the input and output signals and only differs from (3) by a few constant phase terms.

B. MMI Coupler Based Switch Optical Schematic

The optical schematic of the cascaded MMI coupler based switch has been introduced in [6], [7]. The basic structure composes of two cascaded MMI couplers with N phase shifters embedded in the middle of them. The phase shifters can be tuned

either thermally or electronically and the tuning mechanism is dependent on the materials of the phase shifters.

However, according to (3), the adjustment of the phase shifter will be extremely complicated. Each of phase shifter within the array will require an individual phase tuning device, which will result in very high cost. Also, the mechanism of tuning is quite complicated, especially when the number of input is large.

To avoid this, we try to simplify the phase tuning principles. If the phase shifters in the middle of the two MMI couplers can be tuned proportionally, the tuning procedure will be greatly simplified, which means the whole array can be tuned using one thermal or electro process, e.g., one electro-voltage controlling circuit which could provide proportional voltages to each of the electrodes. In order to realize this, the schematic is changed into three fixed phase shifter arrays before, between and after the cascaded MMI couplers together with one variable phase shifter array added in the middle of the two MMI couplers. With this approach, we are able to achieve the proportional tuning of the phase shifters within the variable phase shifter array.

It is worth mentioning that the switching device with two MMI couplers and phase shifter arrays can only provide N switching states, and is an N-port selection switch with N input ports, which is different from the traditional N by N matrix switches. To realize a real N by N matrix switch, multiple devices should be used in a cascaded manner. An example of cascaded MMI switch is presented and discussed in the Appendix.

C. Working Principle for the Switch

We place the fixed phase shifter array whose phase shift is $((i-1/2)^2\pi)/(4N)$ for ith shift element of the array before and after the MMI couplers. The transfer matrix in (3) will be multiplied by two diagonal matrixes and the updated matrix should have the entry of

$$M_{lk} = j\sqrt{\frac{1}{N}}\exp\left(j\frac{\pi}{4}\right) \times \exp\left((-1)^{l+k}\frac{j(l-1/2)(k-1/2)\pi}{2N}\right). \quad (4)$$

We can neglect the common phase term and (4) becomes

$$M_{lk} = \sqrt{\frac{1}{N}}\exp\left((-1)^{l+k}\frac{j(l-1/2)(k-1/2)\pi}{2N}\right). \quad (5)$$

Hence, the phase difference between the columns of the matrix and their complex conjugates is the odd multiple of the following vector or its complex conjugate

$$\left(-\frac{\pi}{4N}, \frac{3\pi}{4N}, \ldots (-1)^l\frac{(2l-1)\pi}{4N}, \ldots, (-1)^N\frac{(2N-1)\pi}{4N}\right). \quad (6)$$

If we add the variable phase shifter array whose phase shift can be tuned as the negative odd multiple of (6), we can generate a matrix whose rows correspond to the complex conjugate of the columns of matrix $\mathbf{M}$ in (5). The row position within the matrix can be adjusted by proportionally tuning the variable phase shifters, and therefore change the state of the switch. As stated in above, the tunable phase shifters should have the phase-shift proportional to

$$-(2N-1) : -(2N-5) : \cdots : -3 : 1 \cdots : (2N-7) : (2N-3) \quad (7)$$

where the positive phase shift can be changed into the negative one via the following relationship:

$$\theta \rightarrow \theta - 2\pi. \quad (8)$$

By tuning the effective index of the phase shifters, the state of the switch is changed accordingly. The contribution of the variable phase shifter array on the transfer matrix can be described by a diagonal matrix with the diagonal entries as

$$D_{ll}^{(2p+1)} = \exp\left(-j(-1)^l\frac{(l-1/2)\pi}{2N}(2p+1)\right) \quad p = 0 \ldots N-1 \quad (9)$$

where p is an integer. The total transfer matrix of the switch is

$$\mathbf{T} = \mathbf{M}\mathbf{D}^{(2\mathrm{p}+1)}\mathbf{M}. \quad (10)$$

The matrix $\mathbf{M}\mathbf{D}^{(2\mathrm{p}+1)}$ can be regarded as a new matrix $\mathbf{N}$ with the entry of

$$N_{kl} = \sqrt{\frac{1}{N}} \times \exp\left((-1)^l\frac{j(l-1/2)(-2p-1+(-1)^k(k-1/2))\pi}{2N}\right). \quad (11)$$

The $\mathbf{N}$ and $\mathbf{M}$ have the relationship seen in (12) at the bottom of the page, where $\bar{\mathbf{M}}$ denotes the transpose of the complex conjugate of $\mathbf{M}$. Equation (12) indicates that the columns of $\mathbf{N}$ are actually the transpose of the corresponding rows of matrix $\mathbf{M}$ (by a phase difference of $\pi/2$ if k is odd and $k+2p+1 > N$ or k is even and $k > 2p+1$). Since $\mathbf{M}$ is a unitary matrix, if one of its rows is multiplied with one of the columns of its transpose, the result will be one if the number of the row and the number of the column are the same, and will be zero otherwise. This is obvious, because transpose of the transfer matrix indicates exchange of input and the output vectors. During the operation

$$N_{kl} = \begin{cases} \bar{M}_{l,2p+1+k} & k \text{ is odd } (k+2p+1 < N) \\ j\bar{M}_{l,2N-2p-k} & k \text{ is odd } (k+2p+1 > N) \\ \bar{M}_{l,2p+2-k} & k \text{ is even } (k < 2p+1 \text{ and } 2p+1-k < N) \\ j\bar{M}_{l,2N-2p-1+k} & k \text{ is even } (2p+1-k > N) \\ \bar{M}_{l,k-(2p+1)} & k \text{ is even } (k > 2p+1) \end{cases} \quad (12)$$

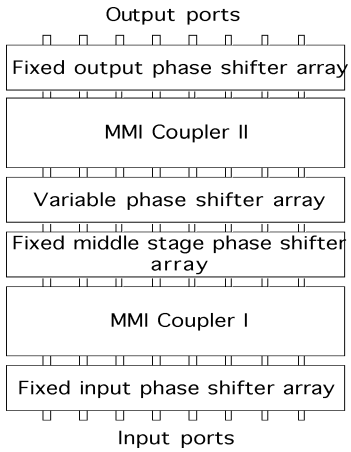

Fig. 1. Optical schematic of the two-stage MMI coupler based switch.

of the device, $\mathbf{M}$ is a fixed matrix, while $\mathbf{N}$ is a variable matrix whose rows are interchanged with the change of p. Their product matrix $\mathbf{T}$ will change accordingly with the element of (13), shown at the bottom of the page, where δ_{ij} is 1 when $i = j$ and is 0 when $i \neq j$. According to (13), $\mathbf{T}$ is a matrix with only one nonzero element in one row or one column. By tuning p, the element of $\mathbf{T}$ and the state of the switch is changed.

It can be concluded that if the signal is injected into the kth input port of the first MMI coupler, the output wave will be expected to appear at the output port of the second MMI coupler whose port number is indicated by the subscript in (12)–(13). By adjusting the integer p, total N states of the switch can be realized.

The optical schematic of the device is illustrated in Fig. 1. It should be noted that the fixed phase shifter array at the output port of the first MMI coupler and the one at the input of the second MMI coupler can be combined as one fixed phase shifter array in manufacturing process, as is illustrated in Fig. 1.

D. Example of a 8 × 8 Switch

As an example, we analyze an 8-port selection switch with 8 input ports using the principles described above. According to (5), the transfer matrix $\mathbf{M}$ for one MMI coupler with two fixed phase shifter arrays is shown in (14) at the bottom of the page.

If the variable phase shifter array is placed between the two MMI couplers (both with two fixed phase shifter arrays), the corresponding transfer matrix $\mathbf{T}$ of the whole system can be calculated according to (10). When the phase of each phase shifter within the variable phase shifter array is varying, i.e., the integer p is varying, the matrix $\mathbf{T}$ will vary accordingly. We calculate the matrix $\mathbf{T}$ using (15) with $p = 0$

$$\frac{1}{8}\begin{pmatrix} 0 & 1 & 0 & 0 & 0 & 0 & 0 & 0 \\ 1 & 0 & 0 & 0 & 0 & 0 & 0 & 0 \\ 0 & 0 & 0 & 1 & 0 & 0 & 0 & 0 \\ 0 & 0 & 1 & 0 & 0 & 0 & 0 & 0 \\ 0 & 0 & 0 & 0 & 0 & 1 & 0 & 0 \\ 0 & 0 & 0 & 0 & 1 & 0 & 0 & 0 \\ 0 & 0 & 0 & 0 & 0 & 0 & 0 & 1 \\ 0 & 0 & 0 & 0 & 0 & 0 & 1 & 0 \end{pmatrix}. \tag{15}$$

The matrix $\mathbf{T}$ with $p = 1, 2, 3, 4, 5, 6, 7$ can be derived in the same approach. It can be seen from these equations that there are totally $N = 8$ states for the switch. If the signal is injected into one of the input port and is required to be switched to one specific output port, there exists one state that could switch the signal to that output port. Also the results shown in the above equation verify the correctness of (11)–(13), which means that the output port number can be calculated using the subscripts in (13).

III. Simulation Results and Discussion

We perform numerical simulation to verify the theoretical predications. The aim of the simulation in this section is to demonstrate the validity of the results discussed in the previous

$$T_{ij} = \sum M_{ik}N_{kj} = \begin{cases} \delta_{i,2p+1+j} & j \text{ is odd } (j + 2p + 1 < N) \\ j\delta_{i,2N-2p-j} & j \text{ is odd } (j + 2p + 1 > N) \\ \delta_{i,2p+2-j} & j \text{ is even } (j < 2p + 1 \text{ and } 2p + 1 - j < N) \\ j\delta_{i,2N-2p-1+j} & j \text{ is even } (2p + 1 - j > N) \\ \delta_{i,j-(2p+1)} & j \text{ is even } (j > 2p + 1) \end{cases} \tag{13}$$

$$\sqrt{\frac{1}{8}}\begin{pmatrix} e^{\frac{j\pi}{64}} & e^{-\frac{j3\pi}{64}} & e^{\frac{j5\pi}{64}} & e^{-\frac{j7\pi}{64}} & e^{\frac{j9\pi}{64}} & e^{-\frac{j11\pi}{64}} & e^{\frac{j13\pi}{64}} & e^{-\frac{j15\pi}{64}} \\ e^{-\frac{j3\pi}{64}} & e^{\frac{j9\pi}{64}} & e^{-\frac{j15\pi}{64}} & e^{\frac{j21\pi}{64}} & e^{-\frac{j27\pi}{64}} & e^{\frac{j33\pi}{64}} & e^{-\frac{j39\pi}{64}} & e^{\frac{j45\pi}{64}} \\ e^{\frac{j5\pi}{64}} & e^{-\frac{j15\pi}{64}} & e^{\frac{j25\pi}{64}} & e^{-\frac{j35\pi}{64}} & e^{\frac{j45\pi}{64}} & e^{-\frac{j55\pi}{64}} & e^{\frac{j65\pi}{64}} & e^{-\frac{j75\pi}{64}} \\ e^{-\frac{j7\pi}{64}} & e^{\frac{j21\pi}{64}} & e^{-\frac{j35\pi}{64}} & e^{\frac{j49\pi}{64}} & e^{-\frac{j63\pi}{64}} & e^{\frac{j77\pi}{64}} & e^{-\frac{j91\pi}{64}} & e^{\frac{j105\pi}{64}} \\ e^{\frac{j9\pi}{64}} & e^{-\frac{j27\pi}{64}} & e^{\frac{j45\pi}{64}} & e^{-\frac{j63\pi}{64}} & e^{\frac{j81\pi}{64}} & e^{-\frac{j99\pi}{64}} & e^{\frac{j117\pi}{64}} & e^{-\frac{j135\pi}{64}} \\ e^{-\frac{j11\pi}{64}} & e^{\frac{j33\pi}{64}} & e^{-\frac{j55\pi}{64}} & e^{\frac{j77\pi}{64}} & e^{-\frac{j99\pi}{64}} & e^{\frac{j121\pi}{64}} & e^{-\frac{j143\pi}{64}} & e^{\frac{j165\pi}{64}} \\ e^{\frac{j13\pi}{64}} & e^{-\frac{j39\pi}{64}} & e^{\frac{j65\pi}{64}} & e^{-\frac{j91\pi}{64}} & e^{\frac{j117\pi}{64}} & e^{-\frac{j143\pi}{64}} & e^{\frac{j169\pi}{64}} & e^{-\frac{j195\pi}{64}} \\ e^{-\frac{j15\pi}{64}} & e^{\frac{j45\pi}{64}} & e^{-\frac{j75\pi}{64}} & e^{\frac{j105\pi}{64}} & e^{-\frac{j135\pi}{64}} & e^{\frac{j165\pi}{64}} & e^{-\frac{j195\pi}{64}} & e^{\frac{j225\pi}{64}} \end{pmatrix} \tag{14}$$

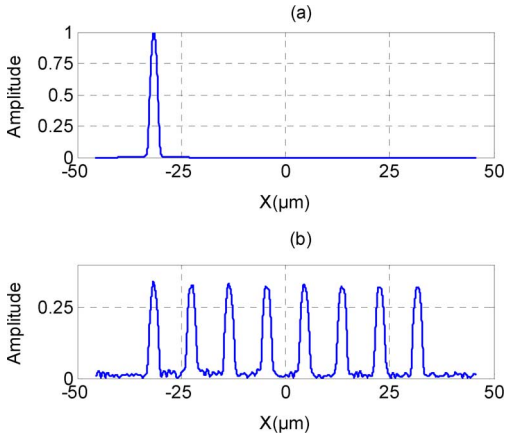

Fig. 2. (a) Input wave amplitude and (b) wave amplitude at the output of the first MMI coupler with the input vector of (1 0 0 0 0 0 0 0).

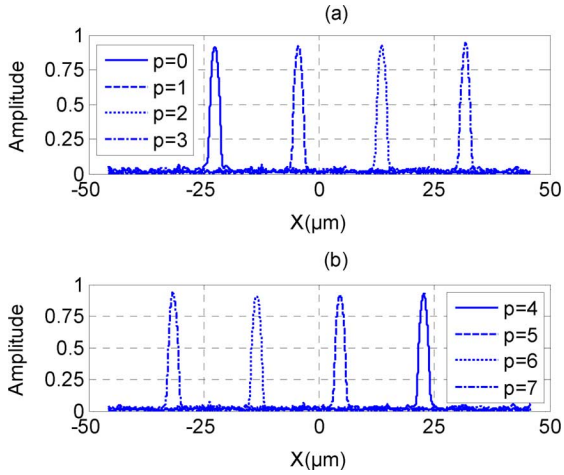

Fig. 3. Wave amplitudes at the output of the second MMI coupler with different middle stage control (with p value varying from 0 to 7) with the input vector of (1 0 0 0 0 0 0 0).

section, to investigate the MMI coupler fabrication error tolerance and to verify the new formulas derived for the phase shifter array fabrication error tolerance analysis. Therefore, the 8×8 optical switch example discussed in the previous section is simulated using 2-D beam propagation method (2DBPM). The switch is composed of six parts: the fixed input phase shift array, the first MMI coupler, the middle stage fixed phase shift array, the middle stage variable phase shift array, the second MMI coupler and the fixed output phase shift array. The phase shift arrays are assumed to be able to provide the exact phase shift described in the previous section and can be realized using the waveguides with different core index. The two MMI couplers are identical with the length of 72 μm. Their core indexes are 3.3989 and the background index is 3.1645, which is from [13]. The effective width of the MMI coupler can be calculated according to [14] with the value of 72.4 μm. The input and the output ports of the MMI coupler are eight identical waveguides with the width of 2.6 μm. The waveguides are connected with the phase shifter arrays. In simulation, the variable phase shifter array is considered to have an equal length of 20 mm, but with slightly different refractive index, which could be induced by the electro-optical or thermal-optical effect. This is in alignment with the configuration mentioned in [8], [15]. It is worth mentioning that, if the phase shifters can be tuned separately, the length of the variable phase shifter could be reduced to a shorter one such as 5 mm, because this length can already provide a phase tuning of 2π [8], [15].

A. Verification of the Operation Principle Proposed in Section II

First of all, we assume the signal is launched to the input port 1 of the device (the input vector is (1 0 0 0 0 0 0 0)). The injected wave amplitude is plotted on the Fig. 2(a). After the interference in the first MMI coupler, the amplitude evolves into the curve in Fig. 2(b). The amplitudes at each of the output ports of the first MMI coupler are equal, which is in accordance with the transfer matrix in (13). The variable phase shift array is tuned to have the odd multiple $(2p + 1)$ of the phase shift vector in (5). With the different odd number $2p+1$, the switch is in a different state accordingly. The wave will appear at the different output port of the second MMI coupler when the state is different, as is indicated by Fig. 3. Fig. 3 is a good illustration for the equations of matrix $\mathbf{T}$ with different p values which were discussed in the previous part. Their first columns indicate the output vectors with the input vector of (1 0 0 0 0 0 0 0) under different tuning number of $2p + 1$. The results match the theoretical prediction in a very precise manner.

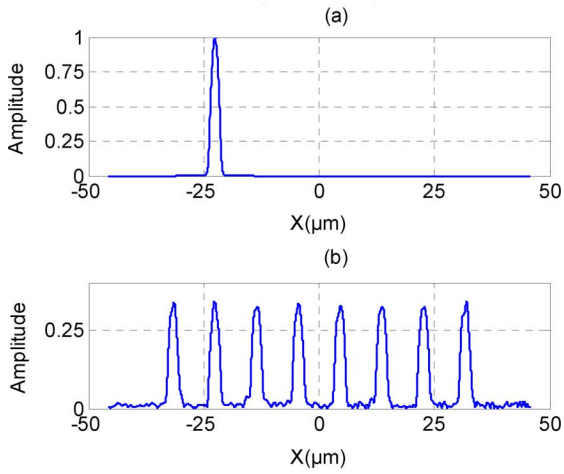

Fig. 4. (a) Input wave amplitude and (b) wave amplitude at the output of the first MMI coupler with the input vector of (0 1 0 0 0 0 0 0).

Secondly, the input vector is changed to (0 1 0 0 0 0 0 0), which is plotted on the Fig. 4(a). Similar to the previous case, the amplitudes have equal amplitudes at each output ports of the first MMI coupler. The variable phase shift array tunes the state of the switch with the change of the tuning number $2p + 1$. The wave at the output ports of the second MMI coupler are plotted on Fig. 5, which agrees with the states of the switch. The directivities of the waves were indicated by the second columns of the matrix $\mathbf{T}$ with different p values. Again, the theory matches the simulation in a very close manner.

B. Fabrication Error Tolerance Analysis of the MMI Coupler

Afterwards, we analyze the fabrication error tolerance of this device. During the analysis, we assume the input vector to be

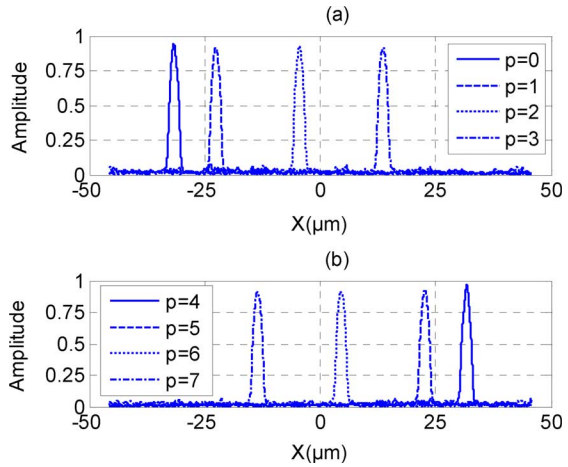

Fig. 5. Wave amplitudes at the output of the second MMI coupler with different middle stage control (with p value varying from 0 to 7) with the input vector of (0 1 0 0 0 0 0 0).

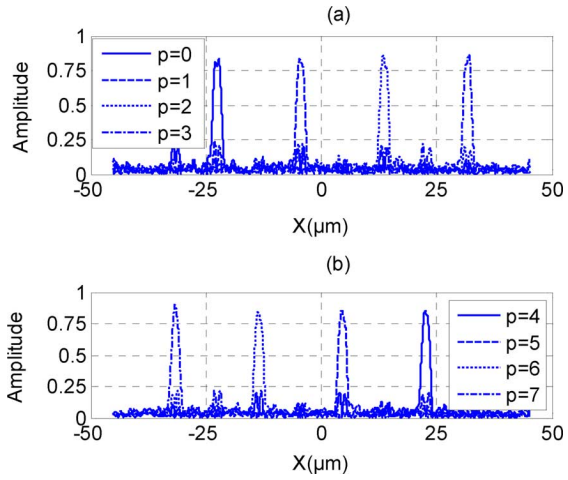

Fig. 6. Output wave amplitude at the output of the second MMI coupler with the input vector of (0 1 0 0 0 0 0 0) and index variation of 0.001.

(1 0 0 0 0 0 0 0). The core indexes of the MMI couplers are assumed to have a variation of 0.001, which could usually happen due to the vertical inaccuracy in the fabrication process. The resulting output curves are shown in Fig. 6. The inaccuracy is about 10% in this case. Furthermore, it can be seen from the figure that the inaccuracy will introduce the crosstalk between the different ports. This phenomenon, however, could be mitigated by making the MMI couplers themselves tunable. Hence, in order to realize a functional MMI coupler switch, thermal or electro tuning materials should also be used for the MMI coupler fabrication as well. The impact of the inaccuracies of the width and length is similar to that of the index deviation. The relationship between them can be derived according to (2) as is indicated in [10].

C. Fabrication Error Tolerance Analysis of the Phase Shifter Arrays

During the fabrication of the device, the inaccuracy may also arise from the phase shifter arrays, which can be analyzed via BPM simulation. However, it is quite a time-consuming task, especially if we consider the manufacturing error to be a random process and want to obtain the important parameters, such as the mean value and the variance of the output error vector. Therefore, an analytical expression describing the impacts of the power imbalance and the phase error of the phase shifter array is presented in this section. The theoretical formula will be verified with the BPM simulation results.

Without loss generality, we focus on the variable inner phase shifter array between the two MMI couplers. The discrepancies arising from the fixed phase shifter arrays can be derived in a similar way and share the similar expressions. The transfer matrix of a device with power balance discrepancy and phase error is

$$\mathbf{T} = \mathbf{M}\mathbf{D}^{2\mathbf{p}+1}\mathbf{D}_E^{2\mathbf{p}+1}\mathbf{A}\mathbf{M} \tag{23}$$

where $\mathbf{A}$ is a diagonal matrix with the diagonal elements whose amplitudes are in the form of $(1 - a_i)$, and $a_1 a_2 \dots a_i \dots$ are positive independent identically distributed random variables indicating the losses of the phase shifter array. $\mathbf{D_E}$ is a diagonal matrix indicating the phase error of the phase shifter array whose phases of the diagonal elements are independent identically distributed random variables with the mean value of 0. In order to verify the proposed model, BPM simulation is performed.

We assume the amplitude vector and phase error vector to be (0.7486 0.994 0.796 0.886 0.751 0.849 0.787 0.871) and $(-3.908\ -6.207\ -6.131\ 3.645\ -3.945\ 0.834\ -6.983\ 3.958)$ (the units for the phase error vector are degree). The input vector is (1 0 0 0 0 0 0 0) and the controlling parameter $p = 0$. According to (23), the calculated output error vector (which is obtained by subtracting the two vectors with and without error) has the amplitudes of (0.067 0.170 0.024 0.029 0.036 0.022 0.041 0.023). From the BPM simulation, the output error vector amplitudes are (0.065 0.166 0.028 0.029 0.035 0.024 0.043 0.022). The results match each other very precisely.

Afterwards, impacts of power imbalance and phase error are studied analytically using (23). Assuming that the input vector is $\mathbf{c}$, the output vector is $\mathbf{b}$, the error vector is $\mathbf{e}$, and we have

$$\begin{aligned} \mathbf{b} &= \mathbf{T}\mathbf{c} \\ \mathbf{e} &= \mathbf{b} - \mathbf{b_0}. \end{aligned} \tag{24}$$

In order to clearly identify which deviation impacts more on the output vector, the impacts of power imbalance and phase error are discussed separately.

Firstly, we consider power imbalance. Since $a_1 a_2 \dots a_i \dots$ are positive independent identically distributed random variables, we have $E(a_i) = E(a_k)$, for all i and k, and the error correlation should be zero when the variables are not identical. Also, it can be derived from (4) that the absolute square of the elements of $\mathbf{M}$ are $1/N$. Based on these assumptions as well as (23) and neglecting the phase error term, the following equation to calculate the mean value and variance of the output error vector can be derived

$$\begin{aligned} E(\mathbf{e}) &= \left(\mathbf{M}\mathbf{D}^{(\mathbf{2p+1})}E(\mathbf{A}-\mathbf{I})\mathbf{M}\right)\mathbf{c} \\ &= \left(\mathbf{M}\mathbf{D}^{(\mathbf{2p+1})}(\mathbf{A_0}-\mathbf{I})\mathbf{M}\right)\mathbf{c} \\ &= -E(a_i)\left(\mathbf{M}\mathbf{D}^{(\mathbf{2p+1})}\mathbf{M}\right)\mathbf{c} \end{aligned}$$

$$= -E(a_i)\mathbf{b}$$
$$\mathrm{Var}(\mathbf{e}) = \mathrm{Var}(a_i) \begin{pmatrix} \frac{1}{N} & \cdots & \frac{1}{N} \\ \vdots & \ddots & \vdots \\ \frac{1}{N} & \cdots & \frac{1}{N} \end{pmatrix} \begin{pmatrix} |c_1|^2 \\ \vdots \\ |c_N|^2 \end{pmatrix} \quad (25)$$

where E denotes the expectation, Var denotes the variance, $\mathbf{A_0}$ denotes the mean value of matrix $\mathbf{A}$. Monte Carlo simulation is performed to verify (25). 10 000 random samples are generated and the resulting output error vectors are calculated using (23). The elements of the power imbalance vector $(a_1\, a_2 \ldots a_N)$ are assumed to be uniformly distributed between the interval [0, 0.3]. The controlling parameter p is assumed to be 4. With the input vector to be (1 0 0 0 0 0 0 0), the output error vector should have the mean value of $(0\ 0\ 0\ 0\ 0\ 0\ -0.15\mathrm{j}\ 0)$ and variance of (0.00094 0.00094 0.00094 0.00094 0.00094 0.00094 0.00094 0.00094 0.00094) according to (25). The Monte Carlo simulation match it with the results of $(0\ 0\ 0\ 0\ 0\ 0\ -0.15\mathrm{j}\ 0)$ and (0.00093 0.00094 0.00094 0.00093 0.00096 0.00094 0.00093 0.00096).

Afterwards, the phase error impact is focused. Similarly, we consider the phase error to be independent identically distributed random variables. They have the same probability distribution function and are not correlated. Neglecting the power imbalance term, the mean value and variance of the output error vector are

$$\begin{aligned} E(\mathbf{e}) &= \left(\mathbf{M}\mathbf{D}^{(\mathbf{2p+1})}E\left(\mathbf{D}_E^{\mathbf{2p+1}} - \mathbf{I}\right)\mathbf{M}\right)\mathbf{c} \\ &= (E(\exp(j(2p+1)\theta_i)) - 1)\left(\mathbf{M}\mathbf{D}^{(\mathbf{2p+1})}\mathbf{M}\right)\mathbf{c} \\ &= (E(\exp(j(2p+1)\theta_i)) - 1)\mathbf{b} \\ \mathrm{Var}(\mathbf{e}) &= \mathrm{Var}(\exp(j(2p+1)\theta_i)) \\ &\quad \times \begin{pmatrix} \frac{1}{N} & \cdots & \frac{1}{N} \\ \vdots & \ddots & \vdots \\ \frac{1}{N} & \cdots & \frac{1}{N} \end{pmatrix} \begin{pmatrix} |c_1|^2 \\ \vdots \\ |c_N|^2 \end{pmatrix}. \end{aligned} \quad (26)$$

If the phase deviation is uniformly distributed between the interval $[-\theta_{\mathrm{m}}, \theta_{\mathrm{m}}]$, expressions in (26) can be further simplified as

$$E(\exp(j(2p+1)\theta_i)) = \frac{\sin((2p+1)\theta_m)}{(2p+1)\theta_m}$$
$$\mathrm{Var}(\exp(j(2p+1)\theta_i)) = 1 - \left(\frac{\sin((2p+1)\theta_m)}{(2p+1)\theta_m}\right)^2. \quad (27)$$

Again, Monte Carlo simulation is performed to verify (26), (27) with 10 000 random samples. The phase errors are assumed to be uniformly distributed between the interval $[-\pi/18, \pi/18]$. The controlling parameter p is still 4. With the input vector to be (1 0 0 0 0 0 0 0), the output error vector should have the mean value of $(0\ 0\ 0\ 0\ 0\ 0\ -0.36\ 0)$, and variance of (0.074 0.074 0.074 0.074 0.074 0.074 0.074 0.074) according to (26), (27). The Monte Carlo simulation matches it with the results of $(0\ 0\ 0\ 0\ 0\ 0\ -0.36\ 0)$ and (0.074 0.076 0.074 0.073 0.074 0.074 0.073 0.075).

From the simulations, it can be seen that the mean value of the output error vector is proportional to the output vector, which means the mean value of the output error vector can be regarded as a loss term on the output vector. The real distortion of the input vector can be evaluated by the variance. It can be concluded from simulations that the phase error plays a more significant role. One more significant factor to enhance the phase error impact is that it increases with the increase of the control parameter p. In comparison, the power imbalance impact is less significant in the simulations. Also, it can be seen from (24) that the more the port number is, the lower variance value of output error vectors is. This is because the error has been averaged at the different ports. According to the above analysis, carefully tuning of the phase shifter array is required to achieve the desired performance.

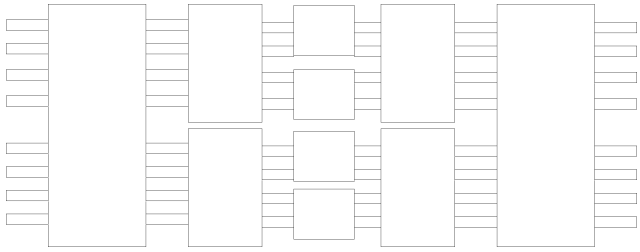

Fig. 7. Optical schematic of the cascaded MMI switch.

Finally, based on (23), and taking into consideration of the contributions of the fixed phase shifter arrays, we simulate the wavelength dependency, which plays a critical role in the device bandwidth evaluation. The center wavelength used in the device design is 1550 nm and in real applications, the wavelength could vary within the C band, i.e., 1530–1565 nm. The simulation shows that wavelength variation within this range will introduce at most -22 dB crosstalk (at the wavelength of 1530 nm and the control parameter $\mathrm{p} = 7$) due to the wavelength/phase variation. How to reduce the wavelength dependency remains an important issue to be studied.

IV. Conclusion

We have analyzed the optical switch based on the MMI couplers and proposed the operation principles for this device based on an analytical transfer matrix theory. An 8×8 MMI coupler based switch is analyzed in detail, which demonstrates the feasibility of the proposed operation principles. The theoretical prediction is verified by the numerical simulations. Fabrication error tolerance analysis is provided afterwards. The design principles presented here can be used for the design of the integrated MMI coupler based switches with either thermal-optical or electro-optical index tuning.

Appendix

In real applications, switches are usually required to be used in a hitless fashion, which means the switching of two input signals should not affect the directivity of others. In this Appendix, we present an example of realization of a hitless switch using the cascaded structure. The optical schematic is illustrated in Fig. 7.

The structure is analogous to the structure proposed for the 4×4 hitless MMI switch proposed in [7]. It is composed of two 8-port MMI switches, four 4-port MMI switches and four 2-port switches. The corresponding controlling parameters are

TABLE AI
CONTROL PARAMETERS SET TO ACHIEVE SWTICHING BETWEEN PORT 3 AND PORT 5

Control parameters	Value
p8_1	7
p8_2:	7
p4_1	3
p4_2	3
p4_3	3
p4_4	3
p2_1	1
p2_2	0
p2_3	1
p2_4	1

p8_1, p8_2, p4_1, p4_2, p4_3, p4_4, p2_1, p2_2, p2_3, and p2_4. The total transfer matrix of the switch can be written as

$$\begin{aligned}\mathbf{T_{total}} = \mathbf{T_{8\_1}} &\begin{pmatrix} \mathbf{T_{4\_1}} & \mathbf{0} \\ \mathbf{0} & \mathbf{T_{4\_2}} \end{pmatrix} \\ &\times \begin{pmatrix} \mathbf{T_{2\_1}} & \mathbf{0} & \mathbf{0} & \mathbf{0} \\ \mathbf{0} & \mathbf{T_{2\_2}} & \mathbf{0} & \mathbf{0} \\ \mathbf{0} & \mathbf{0} & \mathbf{T_{2\_3}} & \mathbf{0} \\ \mathbf{0} & \mathbf{0} & \mathbf{0} & \mathbf{T_{2\_4}} \end{pmatrix} \\ &\times \begin{pmatrix} \mathbf{T_{4\_3}} & \mathbf{0} \\ \mathbf{0} & \mathbf{T_{4\_4}} \end{pmatrix} \mathbf{T_{8\_2}}. \end{aligned} \tag{A1}$$

There are totally ten control parameters to control the state of the switch. Assuming that the input port number is n_{in} and the output port number is n_{out} and the control parameters set is a vector $\mathbf{p} = (\text{p8\_1}, \text{p8\_2}, \text{p4\_1}, \text{p4\_2}, \text{p4\_3}, \text{p4\_4}, \text{p2\_1}, \text{p2\_2}, \text{p2\_3}, \text{p2\_4})$, the directivity of the switching matrix can be described by the following formula:

$$n_{\text{out}} = f(\mathbf{p}, n_{\text{in}}) \tag{A2}$$

where f is the function converting an integer number between [1, N] to another integer within the interval. The function operates according to (13) and (A1). If one needs to find a configuration of $\mathbf{p}$, which switches input n_i and n_j in a hitless manner, the following equation needs to be solved:

$$\begin{cases} n_j = f(\mathbf{p}, n_i) \\ n_i = f(\mathbf{p}, n_j) \\ n_k = f(\mathbf{p}, n_k) \quad k \neq i, j. \end{cases} \tag{A3}$$

By solving $\mathbf{p}$ from (A3), the control parameters are known.

By using the exhaustive searching method to solve (A3) (via a computer program), we have verified that there is always a control parameters set that allows the switching of the two input signals while others remain unswitched. For instance, if we want to switch input port 3 and input port 5, we can set the control parameters as seen in Table AI.

It is worth mentioning that the structure proposed here might not be the optimal configuration to realize a hitless switch. The research on the method to simplify the structure and a faster algorithm to solve (A3) is under way.

ACKNOWLEDGMENT

The authors would like to thank the anonymous reviewers for their rigorous comments during the revision of this contribution.

REFERENCES

[1] G. Zhu and G.-S. Kuo, "A novel integrated multistage 2-D MEMS optical switch with spanke-benes architecture," *J. Lightw. Technol.*, vol. 26, no. 5, pp. 560–568, Mar. 1, 2008.

[2] E. Gros and L. Dupont, "Ferroelectric liquid crystal optical waveguide switches using the double-refraction effect," *IEEE Photon. Technol. Lett.*, vol. 13, no. 2, pp. 115–117, Feb. 2001.

[3] M. M. Vaez and C.-T. Lea, "Strictly nonblocking directional-coupler-based switching networks under crosstalk constraint," *IEEE Trans. Commun.*, vol. 48, no. 2, pp. 316–323, Feb. 2000.

[4] D. K. Cheng, Y. Liu, and G. J. Sonek, "Optical switch based on thermally-activated dye-doped biomolecular thin films," *IEEE Photon. Technol. Lett.*, vol. 7, no. 4, pp. 366–368, Apr. 1995.

[5] F. Wang, J. Yang, L. Chen, X. Jiang, and M. Wang, "Optical switch based on multimode interference coupler," *IEEE Photon. Technol. Lett.*, vol. 18, no. 2, pp. 421–423, Jan. 15, 2006.

[6] L. Cahill, "The modelling of MMI devices," in *Proc. Int. Conf. Transparent Opt. Netw.*, 2006, pp. 138–141.

[7] L. Cahill, "Optical switching using cascaded generalised Mach-Zehnder switches," in *TENCON*, 2005, pp. 1–5.

[8] R. M. Jenkins, J. M. Heaton, D. R. Wight, J. T. Parker, J. C. H. Birbeck, G. W. Smith, and K. P. Hilton, "Novel 1 × N and N × N integrated optical switches using self-imaging multimode GaAs/AIGaAs waveguides," *Appl. Phys. Lett.*, vol. 64, no. 6, pp. 684–686, 1994.

[9] J. Zhou, "Realization of discrete Fourier transform and inverse discrete fourier transform on one single multimode interference coupler," *IEEE Photon. Technol. Lett.*, vol. 23, no. 5, pp. 302–304, Mar. 1, 2011.

[10] A. R. Gupta, K. Tsutsumi, and J. Nakayama, "Synthesis of hadamard transformers by use of multimode interference optical waveguides," *Appl. Opt.*, vol. 42, pp. 2730–2738, 2003.

[11] J. M. Heaton and R. M. Jenkins, "General matrix theory of self-imaging in multimode interference (MMI) couplers," *IEEE Photon. Technol. Lett.*, vol. 11, no. 2, pp. 212–214, Feb. 1999.

[12] M. Bachmann, P. A. Besse, and H. Melchior, "General self-imaging properties in N*N multimode interference couplers including phase relations," *Appl. Opt.*, vol. 33, pp. 3905–3911, 1994.

[13] M. Rajarajan, B. M. A. Rahman, T. Wongcharoen, and K. T. V. Grattan, "Accurate analysis of MMI devices with two dimensional confinement," *J. Lightw. Technol.*, vol. 14, no. 9, pp. 2078–2084, Sep. 1996.

[14] L. B. Soldano and E. C. M. Pennings, "Optical multimode interference devices based on self-imaging: Principles and applications," *J. Lightw. Technol.*, vol. 13, no. 4, pp. 615–627, Apr. 1995.

[15] L. Babaud, F. H. Groen1, X. J. M. Leijtens1, M. Bertogna, J. H. den Besten, Y. Barbarin, Y. S. Oei1, F. Karouta1, J. J. M. Binsma, and M. K. Smit, "First integrated continuously tunable AWG-based laser using electro-optical phase shifters," in *Proc. 12th Eur. Conf. Integrated Opt. (ECIO)*, Grenoble, France, Apr. 6–8, 2005, pp. 156–159.

Author biographies not included at author request due to space constraints.